Multiple verification in complex biological systems: the bone remodelling case study

Ezio Bartocci[1], Pietro Liò[2], Emanuela Merelli[3], and Nicola Paoletti[3]

[1] Department of Computer Engineering, Vienna University of Technology, AT
[2] Computer Laboratory, University of Cambridge, UK
[3] School of Science and Technology, Computer Science Division
University of Camerino, IT

Abstract. We present a set of formal techniques and a methodology for a composite formal analysis at the tissue and organ levels, focusing on the verification of quantitative properties in the process of bone remodelling. Starting from a differential equation model, we derive a stochastic model and a piecewise-multiaffine approximation in order to perform model checking of stabilisation properties for the biological tissue, and to assess the differences between a regular remodelling activity and a defective activity typical of pathologies like osteoporosis. The complex nonlinear dynamics of bone remodelling is analysed with a variety of techniques: sensitivity analysis for the differential equation model; quantitative probabilistic model checking for the stochastic model; and classical model checking and parameter synthesis on the piecewise-multiaffine model. Such analyses allow us to extract a wealth of information that is not only useful for a deeper understanding of the biological process but also towards medical diagnoses.

Keywords: formal analysis, bone remodelling, model checking, sensitivity, piecewise-multiaffine abstraction

1 Introduction

The emergence of new computational frameworks [13, 16, 24, 6, 17] that enable the formal analysis of complex biological systems with stochastic [13], ordinary differential equations [17, 6, 24] and hybrid semantics [10, 9, 6] has changed cell biology from a pure wet lab-based science to also an engineering and information science. In this paper, similar in spirit to [1], we present a set of formal techniques and a methodology suitable to specify and analyse bone remodelling, a system which is representative of a variety of physiological processes characterized by a multiscale interplay between different populations of cells that regulate together tissue homeostasis.

We give a mesoscopic description of the bone remodelling process, able to capture the essential features leading to tissue phenotype changes and to the emerging of a disease condition. Starting from a mathematical continuous model, we implement different encodings for deriving a stochastic model and a piecewise-multiaffine discrete abstraction, in order to tackle the complexity of the bone

remodelling system with formal analysis methods like sensitivity analysis, quantitative verification and parameter synthesis.

1.1 Bone remodelling as a paradigm for organ functional maintenance

Bone remodelling (BR) is a process iterating throughout life, by which aged bone is continuously renewed in a balanced alternation of bone resorption (performed by cells called *osteoclasts*) and formation (performed by *osteoblasts*). It is responsible for repairing micro-damages, for maintaining mineral homeostasis and for the structural adaptation of bone in response to mechanical stress. In other words, a regular remodelling activity ensures the mechanical quality of the bone. Pathologies arise when the resorption and the formation phases are not in equilibrium: osteoporosis is an example of negative remodelling where resorption prevails on formation. In this situation even small negative changes in bone density become more and more critical as subsequent remodelling iterations follow one another.

Osteoclasts and osteoblasts form together the so-called *Basic Multi-cellular Units (BMUs)*, and their dynamics is prominently regulated by the *RANK/ RANKL/OPG signalling*. RANK is a protein expressed by osteoclasts, and acts as a receptor for RANKL, a protein produced by pre-osteoblasts. RANK/RANKL signalling triggers osteoclast differentiation, proliferation and activation, thus it strongly affects the resorption phase and consequently the bone metabolism. Osteoprotegerin (OPG) is a decoy receptor for RANKL. It is expressed by mature osteoblasts and it binds with RANKL, thus inhibiting the production of osteoclasts and protecting in this way bone from excessive resorption.

Bone remodelling can be seen as a paradigm for several other physiological systems, since similarly to the epithelium renewal process, the haematopoiesis process and many others, it is characterized by a birth-death dynamics involving different populations of cells (osteoclasts and osteoblasts) which together contribute in maintaining the stability of the tissue level and of the organ level. Furthermore, bone remodelling is a multiscale process where the molecular scale affects the cellular scale (e.g. RANKL induces osteoclasts' proliferation), and in turn the cellular scale affects the tissue scale (the number and the activity of bone cells determine tissue density and micro-structure).

The key events occurring during a remodelling cycle are depicted in Fig. 1 and can be summarized as follows:

- **Osteoclast recruitment.** Pre-osteoblasts divide and differentiate from stromal cells. They start to express RANKL, attracting pre-osteoclasts, which have RANK receptors on their surfaces. RANK/RANKL signalling triggers pre-osteoclasts' proliferation and differentiation.
- **Resorption.** The pre-osteoclasts enlarge and fuse into mature osteoclasts, that subsequently attach to the bone surface, consuming it. After the resorption process has terminated, osteoclasts undergo apoptosis.

– **Osteoblast recruitment.** Pre-osteoblasts mature into osteoblasts and start producing OPG. OPG inhibits RANKL expression, and consequently protects bone from excessive resorption since it avoids other osteoclasts to be recruited by RANK/RANKL binding.
– **Formation.** Osteoblasts secrete layers of osteoids until the cavity has been filled.

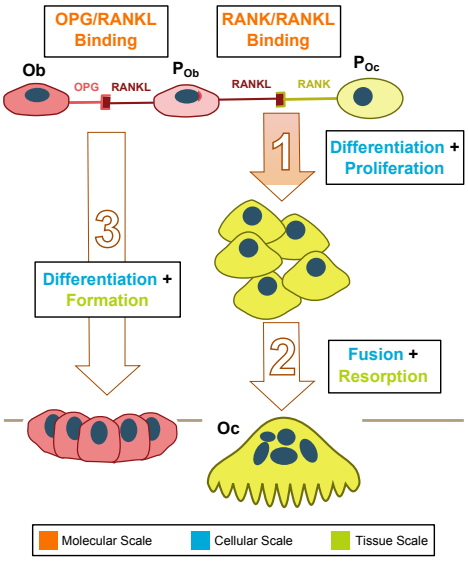

Fig. 1. Multiscale dynamics in bone remodelling. RANK/RANKL signalling triggers osteoclasts' differentiation and proliferation. RANKL/OPG binding inhibits osteoclasts' recruitment and induces osteoblasts' maturation. Bone cells are responsible for tissue turnover.

1.2 Computational bone remodelling

In the last twenty years, a variety of mathematical models has been proposed in order to better understand the dynamics of bone remodelling (reviewed in [19, 18, 35]). Earlier models were focused on the organ level, providing a coarse-grained description of bone as a continuum material only characterized by its density, thus ignoring micro-structural information and cellular dynamics. More detailed models consider biomechanical aspects of the bone tissue for understanding how mechanical loading affects the tissue structure and consequently its function [41]. The description of bone remodelling that we provide in this paper can be classified in another category, that focus on the population dynamics of bone cells. These models describe the single-cellular and multi-cellular level and the interactions occurring among the different types of bone cells involved in the BR

process. They study the continuous variations in the number of bone cells, and the bone density is usually calculated as a function of the number of osteoblasts and osteoclasts and their formation and resorption rates. Although most of such models rely on continuous mathematics, several computational models for bone remodelling have been proposed, including cellular automata [40], Petri Nets [27], membrane systems [11], process algebra and agent-based models [31, 32], stochastic modelling and probabilistic verification [29].

1.3 Formal analysis of bone remodelling dynamics

In this paper we aim to investigate and compare different formal techniques for the analysis of the complex dynamics of the bone remodelling system. Figure 2 summarizes the methodological approach followed. Three different models for BR are provided:

- **ODE model.** It describes the continuous changes of, and the interactions between osteoclasts and osteoblast. Bone density is given by the difference between the formation activity (proportional to osteoblasts concentration) and the resorption activity (proportional to osteoclasts concentration). Besides numerical simulations of the system and the analytical solution of steady states, *sensitivity analysis* [38] is used for evaluating the effects on the system when parameters vary over large ranges.
- **Stochastic model.** We define a stochastic model from the ODE specification, for reasoning on the random fluctuations and the discrete changes of bone density and bone cells. After showing a good fitting between the continuous model and the expected values of the stochastic one, we employ *probabilistic model checking* for giving precise quantitative insights into the system.
- **Piecewise-multiaffine (PMA) model.** We derive an optimal PMA approximation of the ODE model, following the approach presented in [21]. This class of hybrid systems provides a suitable discrete abstraction of the reachable sets and their possible trajectories over which classical *model checking* and *parameter synthesis* techniques can be applied.

This pipeline of models and analysis methods has been developed with the aim to assess two crucial properties in the bone remodelling system from multiple methodological viewpoints:

- **Defective bone dynamics.** We simulate pathologies characterized by bone loss and structural deterioration like osteoporosis, by tuning the death rates of osteoclasts and osteoblasts. This gives rise to a couple of parameter configurations: a *control* configuration (regular death rates and bone activity); and an *osteoporotic* configuration (increased death rates and lossy bone activity).
- **Stabilisation.** It is a crucial property in our system as well as in a broad class of biological examples. Indeed the stabilisation of bone density to its initial level is a desirable feature, since it underlies tissue homeostasis and

therefore the correct functioning of the whole skeleton. In turn bone stabilisation strongly depends on the balanced alternation, and consequently on the stabilisation of osteoclasts and osteoblasts at the end of their resorption and formation activity, respectively. In many cases stabilisation is defined as the existence of a unique fixpoint state that is always eventually reached [14]. In this work we prove stabilisation-related properties that are:

1. Robustness of stabilisation with respect to initial conditions (ODE and stochastic model)
2. Down-regulation of osteoclasts by osteoblasts (stochastic and PMA model)
3. Boundedness of osteoclasts and osteoblasts (PMA model)

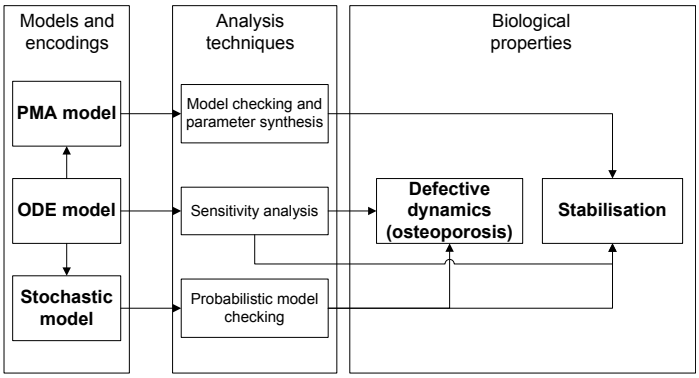

Fig. 2. Multiple formal analysis. The leftmost column displays the different models used and their mutual encodings. The central column lists the used techniques. The rightmost column shows the biological properties under analysis.

The remainder of the paper is organized as follows. In Section 2 we present the ODE model for bone remodelling. In Section 3 we encode its stochastic counterpart and perform quantitative analysis over the model variables. Section 4 illustrates how to derive the piecewise-multiaffine abstraction. In Section 5 the results of formal analysis of defective bone dynamics and stabilisation are shown. Conclusions are given in Section 6.

2 ODE model

In this part we define a continuous mathematical model for cellular bone remodelling adapted from [23]. It describes the temporal changes in osteoclast (x_1) and osteoblast (x_2) populations in a BMU and the resulting bone density (z) as a function of the concentrations of x_1 and x_2.

$$\dot{x_1} = \alpha_1 x_1^{g_{11}} x_2^{g_{21}} - \beta_1 x_1 \tag{1}$$

$$\dot{x_2} = \alpha_2 x_1^{g_{12}} x_2^{g_{22}} - \beta_2 x_2 \tag{2}$$

$$\dot{z} = -k_1 x_1 + k_2 x_2. \tag{3}$$

Model parameters (listed in Table 1) have been calibrated so that variables x_1 and x_2 represent the actual number of osteoclasts and osteoblasts in a BMU. Recent experimental evidences based on the measurement of bone cells surfaces [34] suggest that in control subjects the ratio between osteoblasts and osteoclasts in a BMU varies around a mean value of 10. Given that the number of osteoclasts during resorption is estimated to 10 [33, 23], we make x_1 and x_2 range in the interval $[0, 10]$ and $[0, 100]$ respectively, as shown in the simulation plots (Fig. 3). Further details on the parameter estimation procedure can be found in Appendix 2 of the Supplemental Material.

The parameters g_{ij} describe the effectiveness of autocrine and paracrine regulation. In the autocrine process the cell signals itself by secreting a chemical that binds with receptors on the surface of the same cell. In the paracrine process a chemical signals that diffuse into the area interacts with receptors on nearby cells. Here g_{11} describes the osteoclast autocrine regulation, g_{22} the osteoblast autocrine regulation, g_{21} is the osteoblast-derived paracrine regulation, and g_{12} is the osteoclast paracrine regulation. The nonlinearities of these equations are approximations for the interactions of the osteoclast and osteoblast populations in the proliferation terms of the equations. As reported in Table 1, the autocrine signalling has a positive feedback on osteoclast production ($g_{11} > 0$), and paracrine signalling has a negative feedback on osteoclast production ($g_{21} < 0$). The autocrine signalling has a positive feedback on osteoblast production ($g_{22} > 0$), while the paracrine signalling does not affect osteoblast production ($g_{12} = 0$).

The resulting relative bone density (z) is calculated as the difference between the formation ($k_2 x_2$) and the resorption ($k_1 x_1$) activity, where k_1 and k_2 are the resorption and formation rates, respectively. The variable z measures the percentage changes in bone density with respect to an initial optimal value, which is set to zero.

The non-trivial steady state solution $(\bar{x_1}, \bar{x_2})$ (obtained analytically by setting $\dot{x_1} = 0$ and $\dot{x_2} = 0$)is given by the equations

$$\bar{x_1} = \left(\frac{\beta_1}{\alpha_1}\right)^{(1-g_{22})/\Gamma} \left(\frac{\beta_2}{\alpha_2}\right)^{g_{21}/\Gamma} \tag{4}$$

$$\bar{x_2} = \left(\frac{\beta_2}{\alpha_2}\right)^{(1-g_{11})/\Gamma} \left(\frac{\beta_1}{\alpha_1}\right)^{g_{12}/\Gamma}, \tag{5}$$

where $\Gamma = g_{12}g_{21} - (1 - g_{11})(1 - g_{22})$. With these parameters, $\bar{x_1} = 1.265 \times 10^{-3}$ and $\bar{x_2} = 2.531 \times 10^{-1}$.

The set of ODEs considered in (1-3) belong to the class of S-Systems described in details in [30]. While the study of the global stability of these nonlinear systems is usually not so straightforward, the local stability around an equilibrium (or steady state) point can be determined from the eigenvalues of Jacobian around the equilibrium point.

Figure 3 depicts the simulation plots for x_1, x_2 and z during a single remodelling cycle (about 400 days). The initiation of a remodelling cycle is modelled with a momentary increase of x_1 from $\bar{x_1}$ at time 0. Osteoclasts' lifespan is much

shorter than osteoblasts, and consistent with experimental data in [33], maximal erosion is reached at $t = 10$ days. Henceforth, osteoblasts mineralize the consumed bone and at about $t = 400$ days, the initial steady level of bone density is achieved (bone homeostasis), and both osteoclasts and osteoblasts reach their stable states.

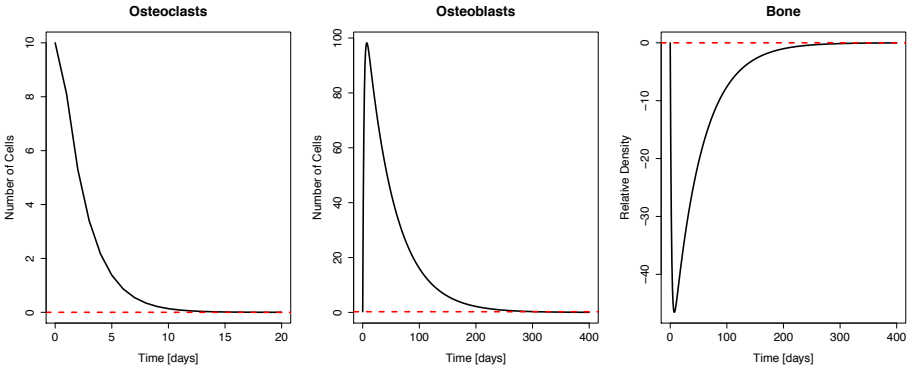

Fig. 3. Simulation results of a single remodelling cycle for x_1, x_2 and z. Dashed lines mark the steady state concentrations for osteoclasts and osteoblasts, and the initial bone density. The remodelling cycle is triggered by an increase in the number of osteoclasts from their steady level, such that the initial conditions are $(x_1^0, x_2^0) = (10{+}\bar{x_1}, \bar{x_2})$. The stabilisation of osteoclasts is achieved at about $t = 20$ days, and at the end of the cycle, we observe the stabilisation of osteoclasts and osteoblasts, and the initial bone density being re-established.

3 Stochastic model for quantitative verification

Randomness and stochasticity are inherent features of biological systems. Living cells are complex mixtures of a variety of complex molecules that are constantly undergoing reactions with one another, and such reactions typically have an exponential distribution associated [20]. Stochasticity plays a key role in bone remodelling, e.g. the fluctuations in molecular concentrations (RANKL and OPG) produce changes in the chemotaxis, that is the process by which cells move toward attractant molecules, of osteoclasts and osteoblasts. This may affect for example the cell differentiation, number and arrival time, and consequently the whole remodelling process. Moreover, autocrine and paracrine regulation among osteoblasts and osteoclasts results from stochastic interactions whose propensity is determined by the availability of a particular class of cells, that are naturally discrete.

Being continuous and deterministic, the ODE model presented in Sect. 2 is not capable to express such crucial aspects. Following and extending the work

Param	Value	Description
α_1	0.5 day^{-1}	Oc growth rate
α_2	4 day^{-1}	Ob growth rate
β_1	0.51 day^{-1}	Oc death rate
β_2	0.02 day^{-1}	Ob death rate
g_{11}	1.1	Oc autocrine regulation
g_{22}	0	Ob autocrine regulation
g_{12}	1	Oc paracrine regulation
g_{21}	-0.5	Ob paracrine regulation
k_1	1.9 cell^{-1} day^{-1}	Resorption rate
k_2	9.48×10^{-3} cell^{-1} day^{-1}	Formation rate
$\mathsf{k}_{\mathsf{ageing}}$	[1, 2]	Ageing factor

Table 1. Model parameters. The ageing factor (k_{ageing}) is responsible to increase the death rate of bone cells (see Sect. 5.1) and varies between 1 (control patient) and 2 (osteoporotic patient). Details on parameter estimation can be found in Appendix 2 of the Supplemental Material.

in [29], we define a stochastic model for bone remodelling and perform formal analysis by means of probabilistic verification techniques, for assessing the probability of a particular configuration of the biological system (usually expressed as a temporal logic property) being reached. In particular, we employ the probabilistic model checker PRISM [26], which has been largely adopted in several biological case studies, especially for modelling biochemical pathways [25, 12, 3, 37]. In this section, we extend this approach to cellular networks, in order to give theoretically justified and quantitative insights in the remodelling process and in the development of defective bone pathologies.

In our settings we use *Continuous Time Markov Chains (CTMC)*, following a *population-based* approach where osteoclasts and osteoblasts are defined as PRISM modules. Each module is equipped with a random state variable modelling the discrete number of cells; and with a list of guarded and stochastic transitions of the form

$$[label]\ guard\ \rightarrow\ rate : update$$

where *label* is an optional transition label; *guard* is a predicate over the state variables determining whether the transition is enabled or not; in the CTMC settings, *rate* is the speed/propensity of the action, giving rise to an exponentially distributed duration of the transition with mean $1/rate$ (faster action have a higher probability of being taken than slower one); and *update* optionally sets new values to state variables.

The PRISM model has been derived from the ODE in Section 2 by applying the following method [15]. Consider a simple ODE population model of the form

$\dot{x} = \alpha - \beta$. The corresponding transitions would be:

$$x < x_{max} \ \rightarrow \alpha : x = x + 1$$
$$x > x_{min} \ \rightarrow \beta : x = x - 1$$

where x_{min} and x_{max} define the range within which the random variable x can vary. In other words, the growth rates in the ODE model become the stochastic rates of "incrementing" transitions, while death rates are involved in the transitions decrementing the population size.

Table 2 summarizes the transitions of osteoclasts and osteoblasts. We do not assume any scaling factor between variables in the continuous model and variables in the stochastic model. Therefore the random variables x_1 and x_2 represent the discrete number of osteoclasts and osteoblasts in a BMU. In order to reduce the state-space of the stochastic model, the relative bone density has not been implemented as a state variable, but as transition rewards, i.e. costs associated to osteoclasts'/osteoblasts' transitions. Further details on the stochastic model and on its implementation in PRISM can be found in Appendix 1 of the Supplemental Materials.

$[\,]$	$0 < x_1 < x_1^{max} \wedge x_2 > 0$	$\rightarrow \alpha_1 x_1^{g_{11}} x_2^{g_{21}}$	:	$x_1 = x_1 + 1$
$[\,]$	$x_1 > 0$	$\rightarrow \beta_1 x_1$	:	$x_1 = x_1 - 1$
$[resorb]$	$x_1 > 0$	$\rightarrow k_1 x_1$	:	$true$

(a) Osteoclasts

$[\,]$	$0 < x_2 < x_2^{max} \wedge x_1 > 0$	$\rightarrow \alpha_2 x_1^{g_{12}} x_2^{g_{22}}$	:	$x_2 = x_2 + 1$
$[\,]$	$x_2 > 0$	$\rightarrow \beta_2 x_2$	:	$x_2 = x_2 - 1$
$[form]$	$x_2 > 0$	$\rightarrow k_2 x_2$	:	$true$

(b) Osteoblasts

$[resorb]\ true\ :\ 1$

(c) Bone resorbed reward

$[form]\ true\ :\ 1$

(d) Bone formed reward

Table 2. Stochastic model for bone remodelling. Guard predicates in osteoblasts and osteoclasts transitions are set in order to avoid out-of-range updates and 0- or infinite-valued transition rates occurring because of nonlinearities in growth and death rates. Maximum values for state variables have been set to $x_1^{max} = 15$ and $x_2^{max} = 150$. Initial values are $x_1^0 = 10$ and $x_2^0 = 1$. The relative bone density is implemented as a pair of bone resorbed/bone formed rewards on osteoclasts'/osteoblasts' transitions. Resorption and formation rates in the ODE model, i.e. $k_1 x_1$ and $k_2 x_2$ respectively, become the stochastic rates of transitions to which the reward structures are associated.

3.1 Analysis of bone density and bone cells properties

Bone cells concentrations and bone density are assessed through the verification of quantitative properties over the defined stochastic model. As opposed to *qualitative* probabilistic model checking that relies on graph-theoretical algorithms for verifying a given property, *quantitative* probabilistic model checking employs numerical methods to compute probability values and rewards [39].

Properties to verify have been formulated in *CSL (Continuous Stochastic Logic)* [2] extended with rewards. The syntax of CSL is given by the following grammar:

$$\phi ::= true \mid a \mid \phi \wedge \phi \mid \neg\phi \mid \mathcal{P}_{\sim p}[\psi] \mid \mathcal{S}_{\sim p}[\psi]$$
$$\psi ::= X\phi \mid \phi \,\mathcal{U}\, \phi \mid \phi \,\mathcal{U}^I \phi$$

where a is an atomic proposition; $\sim \in \{<, \leq, \geq, >\}$ is a relational operator; $p \in [0, 1]$ and I is an interval of $\mathbb{R}$.

State formulas are given by the standard operators from propositional logic: *true*, a (that holds in the states labelled with a), conjunction and negation; and by the probabilistic operators $\mathcal{P}$ and $\mathcal{S}$. The formula $\mathcal{P}_{\sim p}[\psi]$ is true if the probability p' of the path formula ψ being satisfied is such that $p' \sim p$. The formula $\mathcal{S}_{\sim p}[\psi]$ is true if the steady-state probability (i.e. probability in the long run) p' of the path formula ψ being satisfied is such that $p' \sim p$. In addition PRISM supports the expressions $\mathcal{P}_{=?}[\psi]$ and $\mathcal{S}_{=?}[\psi]$ for computing the actual probability of the formula ψ being satisfied.

Path formulas are built over the next state operator X, the until operator $\mathcal{U}$ and the bounded until operator $\mathcal{U}^I$. From a state s, $X\phi$ is true if in the next state ϕ holds. Formula $\phi_1 \,\mathcal{U}\, \phi_2$ is true if ϕ_2 holds at some point from s, and ϕ_1 holds until ϕ_2 holds. Formula $\phi_1 \,\mathcal{U}^I \phi_2$ is true if ϕ_2 holds in the time interval I, and ϕ_1 holds until ϕ_2 holds. The finally operator $\mathcal{F}\phi$ (eventually ϕ holds), the globally operator $\mathcal{G}\phi$ (ϕ is always true), and their bounded variants are derived from the until operator and the bounded until operator as usual: $\mathcal{F}\phi \equiv true \,\mathcal{U}\, \phi$ and $\mathcal{G}\phi \equiv \neg F \neg\phi$. Rewards-related formulas are defined by

$$\mathcal{R}_{\sim r}[\mathcal{I}^{=t}] \mid \mathcal{R}_{\sim r}[\mathcal{C}^{\leq t}] \mid \mathcal{R}_{\sim r}[F\phi] \mid \mathcal{R}_{\sim r}[\mathcal{S}]$$

where $p, t \in \mathbb{R}$, and ϕ is a CSL formula. From a state s, $\mathcal{R}_{\sim r}[\mathcal{I}^{=t}]$ is true if the expected reward at time t satisfies $\sim r$. $\mathcal{R}_{\sim r}[\mathcal{C}^{\leq t}]$ holds if the expected reward cumulated up to time t satisfies $\sim r$. $\mathcal{R}_{\sim r}[\mathcal{F}\phi]$ holds if the expected reward cumulated before ϕ becomes true meets $\sim r$. $\mathcal{R}_{\sim r}[\mathcal{S}]$ is true if the long-run expected reward meets $\sim r$. Similarly to $\mathcal{P}_{=?}$ and $\mathcal{S}_{=?}$, quantitative reward properties can be specified with the expression $\mathcal{R}_{=?}$. For distinguishing among multiple reward structures, we write $\mathcal{R}^{id}$ to indicate the reward identified by id.

The properties that have been verified over the stochastic model for bone remodelling are listed below.

- **Expected bone cells.** In order to compute the expected values of osteoblasts and osteoclasts during the remodelling cycle, we have defined the

following instantaneous reward properties, where *expOc* and *expOb* are the state rewards associated to x_1 and x_2, respectively:

$$E(x_1)(t) : \mathcal{R}^{expOc}_{=?}[\mathcal{I}^{=t}], \quad t = 0, 10, \ldots, 400$$
$$E(x_2)(t) : \mathcal{R}^{expOb}_{=?}[\mathcal{I}^{=t}], \quad t = 0, 10, \ldots, 400.$$

- **Variance of bone cells.** Being the variance of a random variable X equals to $E(X^2) - (E(X))^2$, we have introduced two additional reward structures defined as the expected value of the squared number of osteoclasts (*squaredOc*) and osteoblasts (*squaredOb*). Therefore, the variance is computed with the following properties:

$$\sigma^2(x_1)(t) : (\mathcal{R}^{squaredOc}_{=?}[\mathcal{I}^{=t}]) - (E(x_1)(t))^2, \quad t = 0, 10, \ldots, 400$$
$$\sigma^2(x_2)(t) : (\mathcal{R}^{squaredOb}_{=?}[\mathcal{I}^{=t}]) - (E(x_2)(t))^2, \quad t = 0, 10, \ldots, 400.$$

- **Ranges of the number of cells in a BMU.** Expected minimum and maximum concentrations of osteoclasts and osteoblasts have been verified by using PRISM filters, a particular kind of formulas capable to compute values simultaneously for several states. Filters are of the form $filter(op, prop, states)$, where *op* is the operator characterizing the type of filter, in our case *range*; *prop* is the property being verified; and *states* is the predicate identifying the set of states over which to apply the filter (if *true* it can be omitted). The resulting properties are:

$$filter(range, E(x_1)(t)) \text{ and } filter(range, E(x_2)(t)), \quad t = 0, 10, \ldots, 400.$$

- **Expected relative bone density.** It is calculated as the difference between the cumulative reward for bone formed, and the cumulative reward for bone resorbed:

$$\mathcal{R}^{boneFormed}_{=?}[\mathcal{C}^{\leq t}] - \mathcal{R}^{boneResorbed}_{=?}[\mathcal{C}^{\leq t}], \quad t = 0, 10, \ldots, 400.$$

Figure 4 displays the temporal changes in the expected values, standard deviations and ranges of osteoclasts, osteoblasts and bone density. Transient analysis performed on the stochastic model (reported in Appendix 1 of the Supplemental Material) did not evidenced any particular behaviour like bistability, since transient probability values agree with the computed expectations. Additionally, we have compared the expected quantities of the stochastic model with the results of the differential equation model of Sect. 2 (see Fig. 5). It is possible to observe a satisfying agreement between the two outputs, also confirmed by the low values obtained for the scaled Sum of Squared Residual (SSR) between the ODE and the stochastic variables. Let $M^{ODE}_{k,l}$ and $M^{Stoch}_{k,l}$ be the k-th data point of the variable l in the ODE model and in the stochastic model, respectively. The sum of squared residuals scaled for the number of data points for the variable l is estimated as:

$$SSR_l = \sum_{k=1}^{n_l} \left(\frac{M^{ODE}_{k,l} - M^{Stoch}_{k,l}}{n_l} \right)^2, \tag{6}$$

where n_l is the number of data points for variable l. By calculating the scaled variant of the common (unscaled) SSR, we obtain a measure of fitting independent from the number of data points, that can considerably affect the result of the analysis. The obtained values are: $SSR_{x_1} = 3.64 \times 10^{-3}$; $SSR_{x_2} = 4.89 \times 10^{-1}$; and $SSR_z = 5.05 \times 10^{-2}$.

Therefore the presented model provides a biologically sound and a numerically faithful stochastic extension of the ODE model, and enables at the same time a variety of rigorous quantitative analysis over the bone remodelling system.

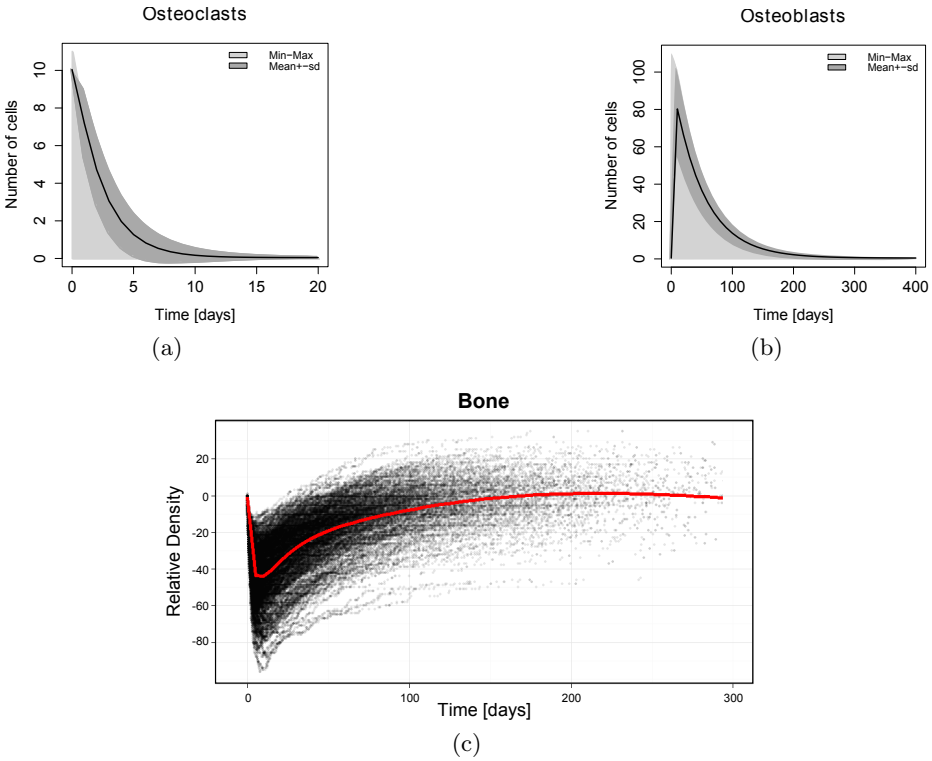

Fig. 4. Stochastic fluctuations in the model variables. Expected values, standard deviation and ranges of bone cells have been computed through the properties in Sect. 3.1. Bone density values have been obtained with 10.000 runs of the PRISM discrete-event simulator.

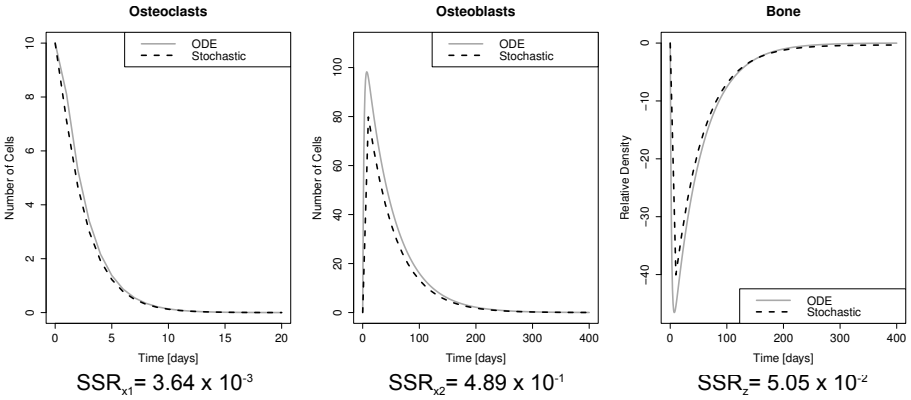

Fig. 5. Comparison between the stochastic model (black dashed curves) and the ODE model (grey continuous curves). A good fitting can be observed between ODE state variables and the expected values of the random variables in the stochastic model, as demonstrated by the scaled sum of squared residuals (SSR) computed between ODE and stochastic variables.

4 Piecewise-multiaffine approximation

The formal analysis of the ODE model presented in Section 2 is intractable due to the presence of the nonlinear terms where the degree of some state variables is greater than one or not even an integer. The stochastic version presented in the previous section is amenable to quantitative analysis only with small concentrations of osteoclasts and osteoblasts, but it suffers the state explosion problem for larger concentrations of these entities.

In the spirit of this paper, we present in this section an alternative method to tackle the problem. Following [21], we have identified a piecewise-multiaffine (PMA) system [7] that best approximates the original one, opening to formal analysis techniques such us model checking [5], reachability analysis [8] and parameter synthesis [6]. This class of hybrid systems, relying on the convexity property [7] of multiaffine functions, provides a conservative overapproximation of the reachable sets represented by hyper-rectangles in the state space. This powerful abstraction results in a discrete transition system, where the states are the reachable sets and the transitions represent the possible trajectories between two reachable sets. A multiaffine function [7] is a polynomial, where the product of different state variables is allowed, but the degree of each state variable is one or zero. We recall the definition of multiaffine function as presented in [8].

Definition 1 (Multiaffine function [8]). *A multiaffine function* $f : \mathbb{R}^n \to \mathbb{R}^n$ *has the following form:*

$$f(x) = \sum_{j=0}^{2^n-1} c_j x_1^{i_1(j)} x_2^{i_2(j)} \cdots x_n^{i_n(j)};\ c_j \in \mathbb{R}^n,$$

where $x = (x_1, \cdots, x_n)$ *and the concatenation* $i_1(j)i_2(j)\cdots i_n(j)$*, with* $\{i_1(j), \cdots, i_n(j)\} \in \{0,1\}^n$*, is a binary representation of the integer* j*.*

In [28] it is shown that any nonlinear function can be approximated with a piecewise-affine function with an arbitrary accuracy and this allows us to re-cast our original model as a PMA. The accuracy of the approximation is not a marginal problem, for example a common question can be: how can we optimally fit the nonlinear terms with a fixed number of segments such that the least square error between the original curve and its approximation is minimum? This issue is solved by a dynamic programming algorithm proposed in [21]: given the sampled points of a set of nonlinear curves representing the dynamics of the system in a particular interval, it finds the optimal global linearisation for a fixed number of segments (or *ramps*) given in input. The resulting PMA identified in a region $[x_1^{min}, x_1^{max}] \times [x_2^{min}, x_2^{max}]$ partitions the concentrations of the osteoclasts and the osteoblasts respectively in ns_1 and ns_2 intervals as it follows:

$$\dot{x_1} = \alpha_1 \sum_{i=1}^{ns_1+1} r(x_1, \theta_i^{(1)}, \theta_{i+1}^{(1)}, y_i^{(1)}, y_{i+1}^{(1)})) \sum_{i=1}^{ns_2+1} r(x_2, \theta_i^{(2)}, \theta_{i+1}^{(2)}, y_i^{(2)}, y_{i+1}^{(2)})) - \beta_1 x_1 \tag{7}$$

$$\dot{x_2} = \alpha_2 x_2 - \beta_2 x_2 \tag{8}$$

$$\dot{z} = -k_1 x_1 + k_2 x_2. \tag{9}$$

with the following thresholds for the state variables x_1 and x_2:

$$\theta_1^{(1)} = x_1^{min} < \theta_2^{(1)} < \cdots < \theta_{ns_1+1}^{(1)} = x_1^{max} \tag{10}$$

$$\theta_1^{(2)} = x_2^{min} < \theta_2^{(2)} < \cdots < \theta_{ns_2+1}^{(2)} = x_2^{max} \tag{11}$$

The higher is the number of chosen intervals, the finer is the resulting abstraction, but the price of precision is the computational time spent in the identification and in the analysis of the system. Figure 6 (a) shows the ramp expression that is formally defined as it follows:

$$r(x, \theta_1, \theta_2, y_1, y_2) = \begin{cases} y_2 & \text{if } x \geq \theta_2 \\ y_1 + (y_2 - y_1)\frac{(x-\theta_1)}{(\theta_2-\theta_1)} & \text{if } \theta_1 \leq x < \theta_2 \\ y_1 & \text{if } x < \theta_1 \end{cases} \tag{12}$$

The sum of ramps is a piecewise-affine function, and the resulting model is piecewise-multiaffine, because the right term of eq. (7) contains the product of two piecewise-affine functions. In the right term of eq. (8), we omit x_1 from the production of the osteoblasts since in the reference model $g_{22} = 0$. The thresholds found after the piecewise-multiaffine model identification partition the state space in hyper-rectangles adjacent and disjointed in which the dynamics is locally multiaffine.

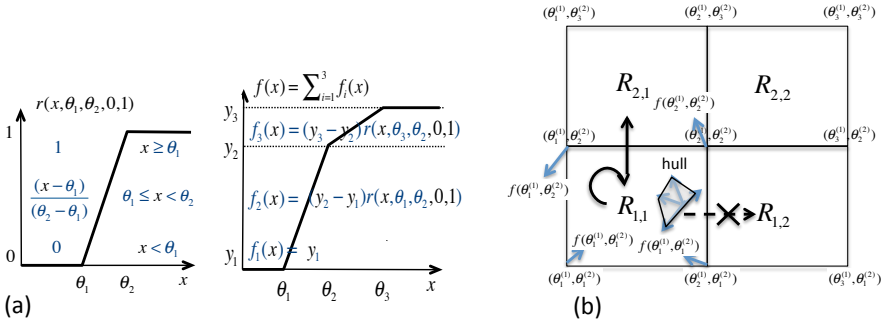

Fig. 6. (a) On the left a single ramp and on the right the sum of two ramps. (b) The convexity property of hyper-rectangles with multiaffine dynamics can be used to determine if there are possible trajectories between two adjacent reachable sets.

Definition 2 (Hyper-rectangle [7]). *For $n \in \mathbb{N}$, a hyper-rectangle R is an n-dimensional rectangle described by:*

$$R = \{x = (x_1, \cdots, x_n) \in \mathbb{R}^n | a_i \leq x_i \leq b_i\}$$

where $a_i, b_i \in \mathbb{R}$, $a_i < b_i$, $i = 1, \cdots, n$.

Proposition 1 (Flow overapproximation [7]). *Let $R \subset \mathbb{R}^n$ a hyper-rectangle, $f_R : R \to \mathbb{R}^n$ be a multiaffine function and $x \in R$. Then $f_R(x)$ is a convex combination of the values of f_R at the 2^n vertices of R.*

This last property is very important to define an abstraction of the PMA system as a discrete transition system. Figure 6 (b) shows an example where a transition between the hyper-rectangles $R_{1,1}$ and $R_{2,1}$ can occur, because the vertical component of $f_{R_{1,1}}$ in one of the two vertices of their facet is greater than zero. A transition cannot instead occur between $R_{1,1}$ and $R_{1,2}$ because the horizontal component of $f_{R_{1,1}}$ in both vertices of their facet is less than zero.

5 Results

5.1 Defective bone remodelling dynamics

We simulate defective dynamics of the remodelling process (i.e. bone negative balance), in order to reproduce bone pathologies like osteoporosis that are characterized by a lower bone density. This negative balance has been modelled by assuming an increased death rate for osteoclasts and osteoblasts, motivated by the fact that the occurrence of defective bone pathologies in elderly patients is partly attributable to the reduced cellular activity typical of those patients. Therefore we have introduced in the ODE model a factor $\mathsf{k}_{\mathsf{ageing}}$ multiplying the

death rates β_i:

$$\dot{x_1} = \alpha_1 x_1^{g_{11}} x_2^{g_{21}} - \mathsf{k}_{\mathsf{ageing}} \beta_1 x_1 \tag{13}$$

$$\dot{x_2} = \alpha_2 x_1^{g_{12}} x_2^{g_{22}} - \mathsf{k}_{\mathsf{ageing}} \beta_2 x_2. \tag{14}$$

In this way we simulate and compare two different classes of patients, i.e. a *control patient* ($\mathsf{k}_{\mathsf{ageing}} = 1$) characterized by a regular bone activity, and an *osteoporotic patient* ($\mathsf{k}_{\mathsf{ageing}} = 2$) characterized by a defective activity and critical bone loss. In Figure 7 the differences in the temporal evolution of bone density are compared under these two configurations considering both the deterministic and the stochastic case. In the osteoporotic case, we observe a lower cellular activity, clearly determined by the increased death rate of cells. An interesting fact is the detection of a bone loss above the 10%, and it is worth noting that in this case the remodelling cycle is faster than in the control configuration. Indeed, the negative balance is reached at about 100 days (1/4 of the regular remodelling time), meaning that the osteoporotic configuration does not determine only a bone density loss, but also a more frequent remodelling activity, leading to a vicious cycle that rapidly weakens the bone density and structure [42]. In order to precisely assess the bone density at the end of the remodelling cycle in the stochastic model, we verify the following formula:

$$\mathcal{R}^{boneFormed}_{=?}[\mathcal{F}\ x_2 = 0] - \mathcal{R}^{boneResorbed}_{=?}[\mathcal{F}\ x_2 = 0], \tag{15}$$

that evaluates the expected relative density cumulated before the number of osteoblasts becomes zero, which indicates the end of the remodelling cycle. The density values obtained by verifying (15) are -0.334 for the control configuration ($\mathsf{k}_{\mathsf{ageing}} = 1$) and -10.593 for the osteoporotic configuration ($\mathsf{k}_{\mathsf{ageing}} = 2$).

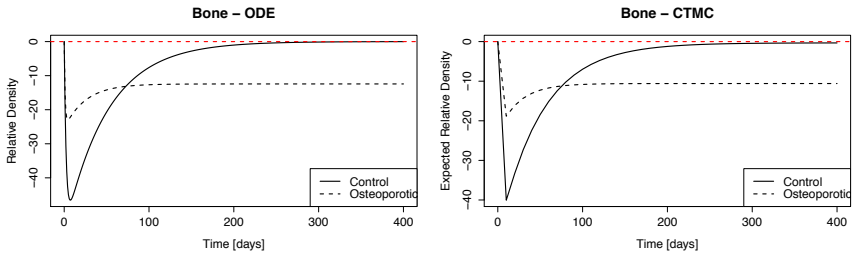

(a) ODE model (b) CTMC model

Fig. 7. Bone density comparison between a control patient ($\mathsf{k}_{\mathsf{ageing}} = 1$) and an osteoporotic patient ($\mathsf{k}_{\mathsf{ageing}} = 2$). In the pathological configuration we observe that bone density varies in a smaller range, which is indicative of a lower cellular activity. Additionally at the end of the remodelling a percentage bone loss greater than the 10% is detected in both the ODE and the CTMC model.

5.2 Analysis of stabilisation properties

Stabilisation is a property of high biological relevance in the bone remodelling system: stabilisation of bone density underlies tissue homeostasis and therefore the maintenance of its mechanical quality. Bone stabilisation depends in turn on the balanced alternation, and consequently on the stabilisation of osteoclasts and osteoblasts at the end of their resorption and formation activity, respectively.

In this part we show the analysis results for the following properties:

1. **Robustness of stabilisation with respect to initial conditions.** Since the starting of a remodelling cycle is simulated by an initial temporary increase of osteoclasts in the BMU, we are interested in assessing how changes in initial concentration of osteoclasts affect remodelling. In particular, we evaluate the effects on the stabilisation of bone cells and bone density, that is normally achieved with the original parameters. This analysis has been performed over the ODE and the stochastic model.
2. **Down-regulation of osteoclasts by osteoblasts.** We verify the effectiveness of the negative regulation that osteoblasts apply on osteoclasts. It is a key feature in the bone remodelling system since it ensures that the resorption phase comes to an end, and consequently that bone is protected from excessive resorption. In other words, we verify that osteoclasts cannot increase when osteoblast concentration is above a given threshold. Additionally we verify the converse property, stating that osteoclasts cannot decrease when the number of osteoblasts is below that threshold. This guarantees that osteoclasts can proliferate in presence of small perturbations of osteoblasts. This analysis has been performed over the PMA and the stochastic model.
3. **Boundedness of osteoclasts and osteoblasts.** We perform parameter synthesis on the piecewise-multiaffine model in order to find regions in the parameter space for which the concentrations of osteoblasts and osteoclasts are below fixed thresholds. The existence of an upper-bound ensures the bounded growth of bone cells and therefore, the absence of anomalous dynamics like the osteoclasts proliferation in bone metastases.

Robustness of stabilisation with respect to initial conditions. Results show that both in the ODE and the stochastic model the stabilisation of x_1, x_2 and z is robust with respect to perturbations in the initial value of x_1 (x_1^0). In other words, homeostasis of bone density and bone cells is maintained regardless the initial concentration of osteoclasts.

In order to assess more formally how x_1^0 affects the remodelling dynamics in the ODE model, global sensitivity analysis [38] has been employed over the three variables of the system. Global sensitivity evaluates the effects on the model output when certain parameters are changed over large ranges. More precisely, parameter values vary in the specified ranges according to some distribution (here uniformly distributed), and the model is run with each of these parameter combinations, for a given number of runs (in this analysis, 100 runs).

In this case we make x_1^0 range in the interval $[\bar{x_1}, 20 + \bar{x_1}]$, where $\bar{x_1}$ is the steady level of osteoclasts analytically solved in Sect. 2 (in the original model,

$x_1^0 = 10 + \bar{x_1}$). As regards the stochastic model, we have computed the expected values of x_1, x_2 and z as explained in Sect. 2, with $x_1^0 = 0, 5, 10, 15, 20$. Figure 8 displays the results and the statistical summary of the three variables at the end of the remodelling cycle.

PMA identification and analysis. We have identified a PMA with 20 intervals for the concentration of the osteoblasts $[0, 2000]$ and 10 intervals for the concentration of the osteoclasts $[0, 15]$. Figure 9 shows a comparison between the original model and the approximated one. The scaled sum of squared residuals (SSR) (see Sect. 3.1) calculated between the ODE and the PMA variables shows a close fit between the two models: $SSR_{x_1} = 6.32 \times 10^{-4}$; $SSR_{x_2} = 5.22 \times 10^{-2}$; and $SSR_z = 1.14 \times 10^{-2}$.

The model obtained has been encoded as a specification for RoVerGeNe[4] [6], a tool designed for robustness analyses and parameters tuning of piecewise-multiaffine differential equation models. Both the robustness analyses and the parameters tuning are guided by the classical model checking, where a property is specified in Linear Temporal Logic (LTL) [36] and the discrete transition system is the abstraction discussed in the previous section. The LTL atomic predicates are of type $(x_i < \theta_j^{(i)})$ or $(x_i > \theta_j^{(i)})$. It supports both logical ($\neg$, $\wedge$, $\vee$) and temporal (X, $\mathcal{U}$, $\mathcal{F}$, $\mathcal{G}$) operators, with the same semantics described for CSL in Section 3.1. In the following, we will use also the implication operator $\rightarrow$, with the usual meaning: $\phi_1 \rightarrow \phi_2 \equiv \neg\phi_1 \vee \phi_2$.

From a formal verification viewpoint, stabilisation is often defined as the existence of a unique fixpoint state that is always eventually reached [14]. Translated into LTL, $\mathcal{F}\mathcal{G}(s)$ must be verified, where s is the global fixpoint/stable state. In our case, since we are more interested in locally stable behaviours, we restrict our analysis only to particular regions (i.e. low/high population of osteoblasts), and we use the following pattern: $p \rightarrow \mathcal{G}(s)$, where p identifies the region of interest in the state space, and s the property that is always verified in that region.

Down-regulation of osteoclasts by osteoblasts. As explained before, we verify that if the population of osteoblasts is greater than the threshold $\theta_3^{(2)} = 2.101$, it will be always true that the population of osteoclasts will not grow, while the osteoblasts remain greater than $\theta_3^{(2)}$. We have verified the robustness of the following LTL property on the PMA system with RoVerGeNe:

$$(x_2 > \theta_3^{(2)}) \rightarrow \mathcal{G}(\wedge_{i=2}^{11}(x_1 < \theta_i^{(1)} \wedge x_2 > \theta_3^{(2)}) \rightarrow X(x_1 < \theta_i^{(1)})).$$

In addition, we demonstrate that the corresponding PRISM property holds also in the stochastic model. We verify the formula

$$\mathcal{P}_{=?}\ [\mathcal{G}((x_1 < \theta^{(1)} \wedge x_2 > \lfloor\theta_3^{(2)}\rfloor) \rightarrow X(x_1 < \theta^{(1)}))],$$

[4] `http://iasi.bu.edu/~batt/rovergene/rovergene.htm`

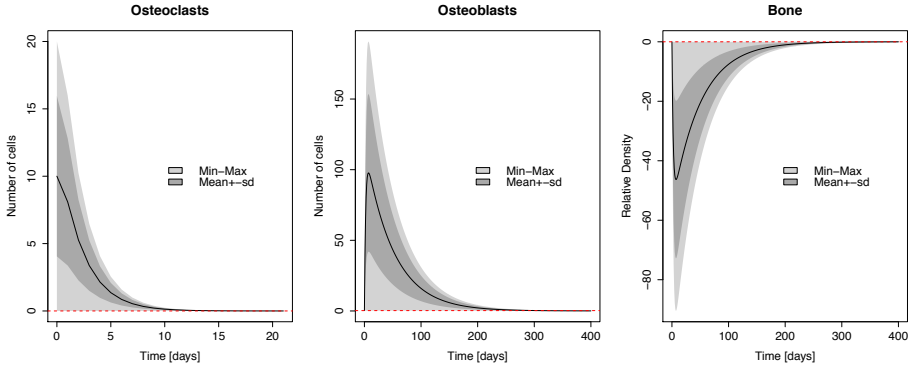

(a)

$(t = 400)$	μ	σ	min	max	$stable$
x_1	7.371×10^{-4}	2.769×10^{-4}	2.75×10^{-4}	1.265×10^{-3}	1.265×10^{-3}
x_2	4.463×10^{-2}	3.711×10^{-2}	2.63×10^{-3}	2.531×10^{-1}	2.531×10^{-1}
z	-1.371×10^{-2}	7.234×10^{-2}	-1.357×10^{-1}	-1.116×10^{-1}	0

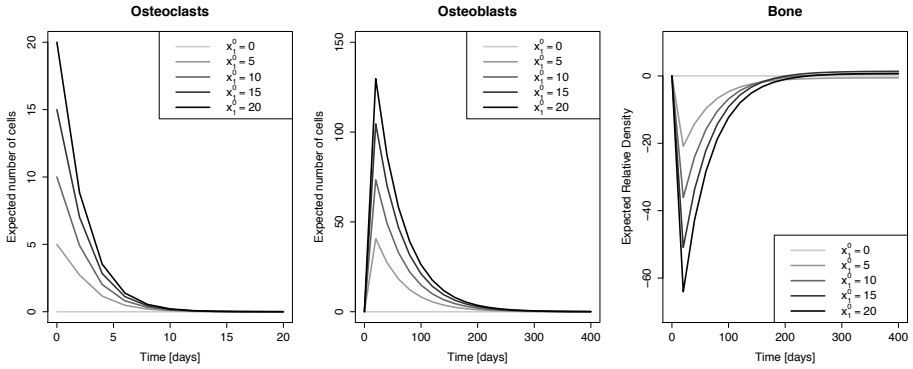

(b)

$(t = 400)$	μ	σ	min	max	$stable$
x_1	1.096×10^{-3}	7.293×10^{-4}	0	1.871×10^{-3}	0
x_2	3.486×10^{-2}	2.568×10^{-2}	0	6.49×10^{-2}	0
z	0.4234	0.736	-0.566	1.366	0

Fig. 8. Stabilisation of the system under perturbations in the initial value of osteoclasts. a) shows the results of the global sensitivity analysis on the ODE model, with $x_1^0 \in [\bar{x_1}, 20 + \bar{x_1}]$ and distributed uniformly. Black curves indicate the mean values μ; dark gray areas indicate the interval $[\mu - \sigma, \mu + \sigma]$; and light gray areas represent the interval between the maximum and the minimum values. b) increasing grey tones show the expected values of the random variables in the stochastic model with $x_1^0 = 0, 5, 10, 15, 20$. The statistical summaries (columns μ, σ, min and max) refer to the variables at the end of the remodelling cycle ($t = 400$ days), and demonstrate that variable values tend or are close to their steady levels (column *stable*).

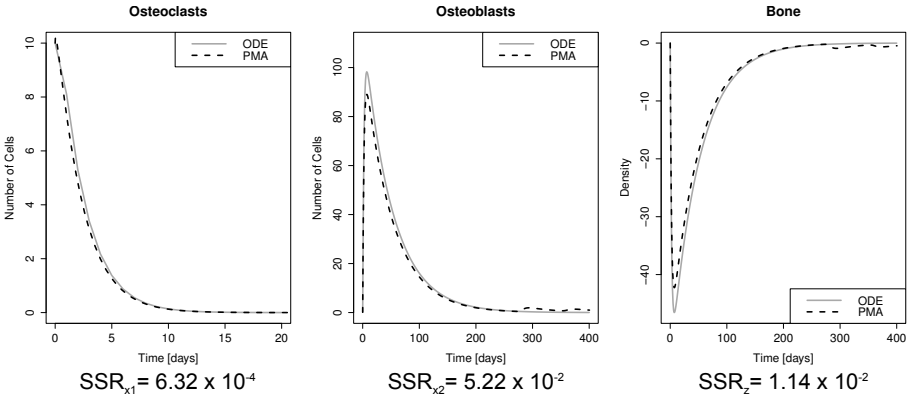

Fig. 9. Comparison between the piecewise-multiaffine model (black dashed curves) and the ODE model (grey continuous curves). In the PMA model, x_1 has been partitioned in 10 intervals: $\theta^{(1)} = \{0.000, 0.413, 1.178, 2.214, 3.482, 4.960, 6.626, 8.472, 10.490, 12.666, 15.000\}$. x_2 has been partitioned in 20 intervals: $\theta^{(2)} = \{0.000, 1.100, 2.101, 3.101, 4.102, 6.103, 9.104, 13.106, 19.109, 28.113, 41.118, 61.127, 90.141, 133.160, 196.188, 289.230, 426.292, 627.382, 923.516, 1358.711, 2000.000\}$. A good fitting can be observed between the ODE and the PMA state variables, as evidenced by their sum of squared residuals (SSR).

which returns a probability value of 1 for each $\theta^{(1)} = 1, \ldots, x_1^{max} = 15$. The attentive reader will notice that the above formula is not CSL, in which temporal operators cannot be combined. The property specification language of PRISM supports also LTL-style path properties, thus making possible to combine temporal operators.

We are also interested in the converse property of down-regulation that is, the proliferation of osteoclasts with small perturbations of osteoblasts. Stated differently we verify that if the population of the osteoblasts is less than $\theta_2^{(2)} = 1.1$, it will be always true that the population of osteoclast will not decrease while the osteoblasts remains lower than $\theta_2^{(2)}$. The LTL formula verified on the PMA system is

$$(x_2 < \theta_2^{(2)}) \rightarrow \mathcal{G}(\wedge_{i=4}^{11}(x_1 > \theta_i^{(1)} \wedge x_2 < \theta_2^{(2)}) \rightarrow X(x_1 > \theta_i^{(1)})).$$

Similarly to the previous case, the proliferation property holds also in the stochastic model. Indeed, the PRISM formula

$$\mathcal{P}_{=?}\ [\mathcal{G}((x_1 > \theta^{(1)} \wedge x_2 < \lfloor \theta_1^{(2)} \rfloor) \rightarrow X(x_1 > \theta^{(1)}))],$$

is exactly true for each $\theta^{(1)} = 1, \ldots, x_1^{max} = 15$.

Boundedness of osteoclasts and osteoblasts. We exploit the parameter synthesis feature of RoVerGeNe in order to find the ranges of parameter for which

the concentrations of osteoclasts and osteoblasts admit a fixed upper bound in the piecewise-multiaffine model. In particular we are interested in tuning the death rates β_1 and β_2 of x_1 and x_2 resp, for which it holds that the population of the osteoclasts is always less than $\theta_{10}^{(1)} = 15$ and the population of the osteoblasts is always less than $\theta_{20}^{(2)} = 2000$. The corresponding LTL property is

$$((x_1 < \theta_{10}^{(1)})) \wedge (x_2 < \theta_{20}^{(2)})) \rightarrow \mathcal{G}((x_1 < \theta_{10}^{(1)})) \wedge (x_2 < \theta_{20}^{(2)})).$$

By making β_1 range in the interval $[0.6, 2.4]$ and β_2 range in $[0.02, 0.08]$, the algorithm for parameter synthesis [6] returns two regions in the parameter space satisfying the boundedness property (see Fig. 10): $2.0381 \leq \beta_1 \leq 2.4 \wedge 0.0373 \leq \beta_2 \leq 0.0454$ and $2.0381 \leq \beta_1 \leq 2.4 \wedge 0.0465 \leq \beta_2 \leq 0.08$.

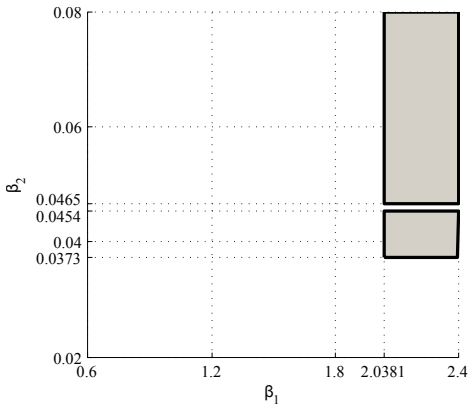

Fig. 10. Parameter synthesis of the formula $((x_1 < \theta_{10}^{(1)})) \wedge (x_2 < \theta_{20}^{(2)})) \rightarrow \mathcal{G}((x_1 < \theta_{10}^{(1)})) \wedge (x_2 < \theta_{20}^{(2)}))$, with $\beta_1 \in [0.6, 2.4]$ and $\beta_2 \in [0.02, 0.08]$. Valid regions are $2.0381 \leq \beta_1 \leq 2.4 \wedge 0.0373 \leq \beta_2 \leq 0.0454$ and $2.0381 \leq \beta_1 \leq 2.4 \wedge 0.0465 \leq \beta_2 \leq 0.08$.

6 Conclusion

We introduced a methodology for checking interesting properties and reasoning about biological systems, focusing on bone remodelling as our case study. We showed how to derive, from the classical ODE model, a stochastic model and a piecewise multiaffine system that best approximates the original one. In the stochastic model the dynamics is locally regulated by the discrete entities (osteoblasts and osteclasts) involved. This model allows us to study the more realistic stochastic fluctuations of the system, but is amenable to quantitative analysis only with small populations of entities, suffering the state explosion problem. In the piecewise multiaffine model the dynamics of the system is governed by hyper-rectangles with locally multiaffine dynamics that partition the

continuous state space. The convexity property of the multiaffine functions provides a powerful abstraction resulting in a discrete transition system, where the states are the reachable sets and the transitions represent possible trajectories between the reachable sets.

Stabilisation properties in a region of the state space can be checked on the models with both the stochastic and the PMA semantics. However, we experienced that the parameter range identification, guided by the satisfaction of stabilisation properties, is infeasible using the techniques nowadays available [22, 4] for the stochastic model, due to the number of the states involved. We showed how this is instead possible in the PMA model using the approach described in [21, 6]. The analysis of the PMA system represents an advantage over the ODEs in terms of behaviour interpretability and provides means to compare parameters with those used in the stochastic model. The combined use of both allows us to identify general trends and variability which could, in future, be associated to disease progression.

From a methodological viewpoint, we address the problem of choosing the most suitable model according to the biological property to analyse and to the formal techniques supported. This work could be also helpful in the area of computational medicine, relatively to the prediction of bone-related diseases and more generally, of diseases where disruptions at the cellular scale affect the stability of the tissue and the organ scales. We showed how defective dynamics like osteoporosis can be simulated with appropriate parameters, and the model could allow us to generate time series of the bone mineral density for specific classes of patients. If we determine the parameter values for a single patient (for instance during a set of medical check-ups) we may be able to predict the bone density at different future times, thus inching towards a practical usefulness in medical diagnoses and treatments.

Acknowledgments The authors thank the anonymous reviewers for helpful comments and constructive suggestions. Nicola Paoletti thanks the EC-funded HPC-Europa2 programme, for supporting his visit to the Edinburgh Parallel Computing Centre (EPCC) and to the Computer Laboratory at the University of Cambridge.

References

1. O. E. Akman, M. L. Guerriero, L. Loewe, and C. Troein. Complementary approaches to understanding the plant circadian clock. In *FBTC*, volume 19 of *EPTCS*, pages 1–19, 2010.
2. A. Aziz, K. Sanwal, V. Singhal, and R. Brayton. Model-checking continuous-time Markov chains. *ACM Transactions on Computational Logic*, 1(1):162–170, 2000.
3. R. Barbuti, S. Cataudella, A. Maggiolo-Schettini, P. Milazzo, and A. Troina. A probabilistic model for molecular systems. *Fundamenta Informaticae*, 67(1-3):13–27, 2005.
4. E. Bartocci, R. Grosu, P. Katsaros, C. Ramakrishnan, and S. Smolka. Model repair for probabilistic systems. In *TACAS*, volume 6605, pages 326–340. Springer, 2011.

5. G. Batt, C. Belta, and R. Weiss. Temporal logic analysis of gene networks under parameter uncertainty. *IEEE Transactions on Automatic Control*, 53:215–229, 2008.
6. G. Batt, B. Yordanov, R. Weiss, and C. Belta. Robustness analysis and tuning of synthetic gene networks. *Bioinformatics*, 23(18):2415–2422, 2007.
7. C. Belta, L. Habets, and V. Kumar. Control of multi-affine systems on rectangles with application to hybrid biomolecular networks. In *Proceedings of the 41st IEEE Conference on Decision and Control*, pages 534–539, 2002.
8. S. Berman, A. Halász, and V. Kumar. MARCO: A reachability algorithm for multi-affine systems with applications to biological systems. In *Proceedings of the 10th International Conference on Hybrid Systems: Computation and Control (HSCC 2007)*, pages 76–89, 2007.
9. L. Bortolussi and A. Policriti. (Hybrid) automata and (stochastic) programs The hybrid automata lattice of a stochastic program. *J Logic Computation*, pages 2052 – 2077, 2010.
10. L. Bortolussi and A. Policriti. Hybrid dynamics of stochastic programs. *Theoretical Computer Science*, 411(20):2052 – 2077, 2010.
11. D. Cacciagrano, F. Corradini, E. Merelli, and L. Tesei. Multiscale Bone Remodelling with Spatial P Systems. In *Proceedings Compendium of the 4th Workshop on Membrane Computing and Biologically Inspired Process Calculi (MeCBIC 2010)*, pages 69–83, 2010.
12. M. Calder, V. Vyshemirsky, D. Gilbert, and R. Orton. Analysis of signalling pathways using continuous time Markov chains. *Transactions on Computational Systems Biology VI*, pages 44–67, 2006.
13. F. Ciocchetta and J. Hillston. Bio-pepa: A framework for the modelling and analysis of biological systems. *Theor. Comput. Sci.*, 410(33-34):3065–3084, 2009.
14. B. Cook, J. Fisher, E. Krepska, and N. Piterman. Proving stabilization of biological systems. In *Proceedings of 12th International Conference on Verification, Model Checking, and Abstract Interpretation (VMCAI 2011)*, pages 134–149, 2011.
15. T. Dayar, L. Mikeev, and V. Wolf. On the numerical analysis of stochastic Lotka-Volterra models. In *Proceedings of the 2010 International Multiconference on Computer Science and Information Technology (IMCSIT)*, pages 289–296, 2010.
16. L. Dematté, C. Priami, and A. Romanel. Modelling and simulation of biological processes in blenx. *SIGMETRICS Perform. Eval. Rev.*, 35(4):32–39, 2008.
17. F. Fages, S. Soliman, and N. Chabrier-Rivier. Modelling and querying interaction networks in the biochemical abstract machine biocham. *Journal of Biological Physics and Chemistry*, 4(2):46–73, 2004.
18. F. Gerhard, D. Webster, G. van Lenthe, and R. Müller. In silico biology of bone modelling and remodelling: adaptation. *Philosophical Transactions of the Royal Society A: Mathematical, Physical and Engineering Sciences*, 367(1895):2011, 2009.
19. L. Geris, J. Vander Sloten, and H. Van Oosterwyck. In silico biology of bone modelling and remodelling: regeneration. *Philosophical Transactions of the Royal Society A: Mathematical, Physical and Engineering Sciences*, 367(1895):2031, 2009.
20. D. Gillespie. Exact stochastic simulation of coupled chemical reactions. *Journal of Physical Chemistry*, 81(25):2340–2361, 1977.
21. R. Grosu, G. Batt, F. Fenton, J. Glimm, C. L. Guernic, S. Smolka, and E. Bartocci. From cardiac cells to genetic regulatory networks. In *Proceedings of the 23rd International Conference on Computer Aided Verification (CAV'11)*, pages 396–411, 2011.
22. E. M. Hahn, H. Hermanns, B. Wachter, and L. Zhang. PARAM: A Model Checker for Parametric Markov Models. In *CAV*, pages 660–664, 2010.

23. S. Komarova, R. Smith, S. Dixon, S. Sims, and L. Wahl. Mathematical model predicts a critical role for osteoclast autocrine regulation in the control of bone remodeling. *Bone*, 33(2):206–215, 2003.
24. J. Krivine, V. Danos, and A. Benecke. Modelling epigenetic information maintenance: A kappa tutorial. In *CAV*, pages 17–32, 2009.
25. M. Kwiatkowska, G. Norman, and D. Parker. Using probabilistic model checking in systems biology. *ACM SIGMETRICS Performance Evaluation Review*, 35(4):14–21, 2008.
26. M. Kwiatkowska, G. Norman, and D. Parker. PRISM 4.0: Verification of probabilistic real-time systems. In *Proceedings of the 23rd International Conference on Computer Aided Verification (CAV'11)*, pages 585–591, 2011.
27. L. Li and H. Yokota. Application of Petri Nets in Bone Remodeling. *Gene Regulation and Systems Biology*, 3:105, 2009.
28. J. Lin and R. Unbehauen. Canonical piecewise-linear approximations. *IEEE Transactions on Circuits and Systems I: Fundamental Theory and Applications*, 39:697–699, 1992.
29. P. Liò, E. Merelli, and N. Paoletti. Multiple verification in computational modeling of bone pathologies. In *Proceedings of the 3rd International Workshop on Computational Models for Cell Processes (CompMod 2011)*, pages 82–96, 2011.
30. E. O. Voit and A. E. Ferreira. *Computational Analysis of Biochemical Systems*. Cambridge University Press, 2000.
31. N. Paoletti, P. Liò, E. Merelli, and M. Viceconti. Osteoporosis: a multiscale modeling viewpoint. In *Proceedings of the 9th International Conference on Computational Methods in Systems Biology (CMSB '11)*, pages 183–193, 2011.
32. N. Paoletti, P. Liò, E. Merelli, and M. Viceconti. Multi-level computational modeling and quantitative analysis of bone remodeling. *IEEE/ACM Transactions on Computational Biology and Bioinformatics*, 99(PrePrints), 2012.
33. A. Parfitt. Osteonal and hemi-osteonal remodeling: The spatial and temporal framework for signal traffic in adult human bone. *Journal of cellular biochemistry*, 55(3):273–286, 1994.
34. M. Parfitt, S. Qiu, S. Palnitkar, and D. Rao. Abnormal bone remodeling in patients with spontaneous painful vertebral fracture. *Journal of Bone and Mineral Research*, 26(3):475–485, 2011.
35. P. Pivonka and S. Komarova. Mathematical modeling in bone biology: From intracellular signaling to tissue mechanics. *Bone*, 47(2):181–189, 2010.
36. A. Pnueli. The temporal logic of programs. In *18th IEEE Annual Symposium on Foundations of Computer Science*, pages 46–57, 1977.
37. T. Pronk, E. de Vink, D. Bošnački, and T. Breit. Stochastic modeling of codon bias with PRISM. In *Proceedings of the 3rd International Workshop Methods and Tools for Coordinating Concurrent, Distributed and Mobile Systems (MTCoord 2007)*, 2007.
38. K. Soetaert, T. Petzoldt, et al. Inverse modelling, sensitivity and monte carlo analysis in R using package FME. *Journal of Statistical Software*, 33(3):1–28, 2010.
39. W. Stewart. *Introduction to the numerical solution of Markov chains*. Princeton University Press NJ, 1994.
40. A. Tovar. *Bone remodeling as a hybrid cellular automaton optimization process*. PhD thesis, University of Notre Dame, 2004.
41. M. Viceconti, L. Bellingeri, L. Cristofolini, and A. Toni. A comparative study on different methods of automatic mesh generation of human femurs. *Medical engineering & physics*, 20(1):1–10, 1998.

42. J. Whitfield. *Growing bone*. Landes Bioscience, 2007.